Wireless Embedded Sensing of Strain and Temperature

DAVID SHAHAN, CONNOR MCMAHAN, CHIA-MING CHANG,
RAYMOND NGUYEN, SOUREN SOUKIAZIAN,
DAVID A. SMITH and TOBIAS SCHAEDLER

ABSTRACT

In this study, we demonstrate the first realization of wireless strain and temperature sensing within 3D-printed metallic structures using standard inspection hardware. This establishes a path toward need-based parts maintenance driven by accurate damage assessments instead of relying on regularly scheduled maintenance teardowns, extending the service intervals of structures operating in harsh environments. To this end, we encapsulate magnetoelastic and thermomagnetic materials inside microtubes and embed the sensing elements mid-print. Mechanical and thermal stimuli affect the magnetic permeability of the embedded materials, which modulates the induced voltage in a coil placed on or near the surface of the printed part. We demonstrate strain sensing accurate to $\pm 25\times10^{-6}$ over a 1×10^{-3} strain range, and temperature sensing accurate to ±0.75˚C over a 70˚C range, both to a 95% confidence interval. This extends non-destructive eddy-current damage detection to accurate, real-time strain and temperature monitoring in aluminum alloys and other metals.

INTRODUCTION

This research seeks to dramatically simplify the overhaul and maintenance of safety critical hardware by enabling in-situ structural integrity measurements in critical locations that are currently only accessible through full disassembly. Traditional strain gauges are limited in their ability to survive operating environments and to access the high stress location. For example, threads and gears experience high stresses at the roots of their teeth respectively, locations that are not available for mounting strain gauges and routing wires to data acquisition hardware. To detect cracks in safety critical hardware, the part often needs to be disassembled and subjected to a fluorescent penetrant inspection (FPI) [1]. Safety critical parts are sized so that the smallest crack detectable via FPI does not propagate to failure in the number of loading cycles between maintenance intervals. Our aim is to embed a sensor as close to the critical stress location as possible without compromising the structural integrity of the part while wirelessly measuring changes in strain and temperature large enough to indicate the presence of damage before part failure. If this can be accomplished by adding low-

HRL Laboratories, LLC. 3011 Malibu Canyon Rd., Malibu, CA 90265

overhead wireless measurement hardware to a routine vehicle functional check, then regular health checks can be done more often, and the expensive inspection teardowns can be performed only on an as-needed basis.

Embedding sensors can be accomplished in a few ways, but here we emphasize the natural application of embedding sensors within 3D printed metal parts. For example, laser powder bed fusion (LPBF) is a viable alternative to conventional machining for fatigue limited parts such as the transmission housing on Boeing's Chinook rotorcraft [2]. 3D printing enables freely placing sensor cavities throughout the volume of the printed part, gaining access to critically stressed locations while protecting the embedded sensor from the harsh operating environment. The printing process can be paused to place the sensing material within the cavity, and resuming the printing process structurally couples the sensing material to the parent material by laser welding it into place. In this paper we show results of successfully embedding sensing material into test specimens made by LPBF using HRL's proprietary aluminum alloy, 7A77 [3]. While improvements are being made on the structural integrity of 3D printed parts, the ability to monitor their stress in-situ may enable more safety critical parts to be 3D printed and the goal of on-demand distributed part production for life-limited critical component spares may be realizable.

Several challenges need to be addressed to be successful. The sensor needs to survive the very high temperatures near the melt pool during the 3D printing process. It needs to be structurally coupled to the parent metal so that it measures part strain once calibrated. The sensor must be accurate over a large enough stress and temperature range to detect changes in stress due to part damage. The smaller the sensor, the closer it can be placed to the location of potential failure without becoming the point of failure. Finally, the sensor needs to be durable since false positives would lead to a premature maintenance check and false negatives would lead to part failure. In this paper we present progress on these requirements except the sensor durability which is currently being tested.

The advantages of our approach, illustrated in Figure 1 for a gear, over other approaches are that our sensors are small and wireless, minimizing our impact on the structure and allowing our sensors to be placed near the point of potential failure without becoming the point of failure. The sensors themselves are embedded magnetoelastic and thermomagnetic materials for strain and temperature sensing respectively. Magnetoelastic materials couple strain to magnetization and thermomagnetic materials couple temperature to magnetization. We measure a change in the sensing material's permeability using electrical coils, called the sensing coils, placed near the part surface. Just like standard eddy current inspection hardware, low frequency AC current in the sensing coils is monitored for changes in impedance, indicating a change in the sensing material's permeability. The primary limitation of our approach is that wireless communication through metal parts has limited range due to eddy current losses in the metal and hence the depth of embedding is limited to less than approximately 25 mm for sensors 10 mm long by 1 mm square cross-sectional area. In this paper, we report results for sensors of this size embedded 2.5 mm deep in 3D printed aluminum test coupons. The embedding depth can be optimized by increasing the power delivered to the sensing coils, optimizing the sensing coils themselves, lowering the AC frequency, or increasing the volume of the embedded sensing material. While wireless sensing has its limitations, the lack of wires reduces the embedded sensor's impact on part integrity

and simplifies monitoring the health of moving hardware such as transmission shafts or rotor blades that would otherwise require a slip ring.

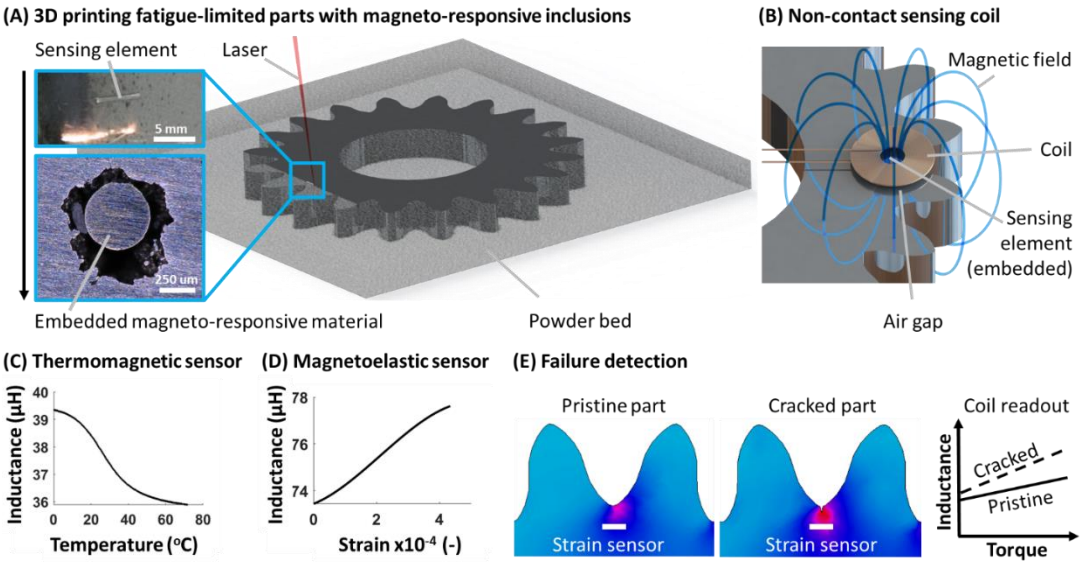

Figure 1. Structural health monitoring approach based on wireless, non-contact strain and temperature sensing using embedded, magneto-responsive materials. (A) Sensing elements containing magnetoelastic or thermomagnetic materials are embedded during additive manufacturing of a fatigue-limited part. (B) Strain and temperature are measured wirelessly by placing AC coils near the part's surface to generate a magnetic field and record the coil inductance, which is modulated by changes in the magneto-responsive materials' permeabilities due to mechanical or thermal effects. (C-D) The magnetic permeability of Monel and Galfenol inclusions change in response to variations in temperature and strain, respectively, modulating the inductance of sensing coils on or near the surface of a part. (E) The initiation of a crack changes the stress field in a gear, modulating the permeability of the magnetoelastic inclusion and therefore the inductance of the sensing coil.

THE SENSING ELEMENTS

We used magnetoelastic Galfenol (FeGa) as the sensing element for strain and thermomagnetic Monel (NiCu) for sensing temperature. The left graph of Figure 2 is a reprint of the publicly available measurement of Galfenol's internal magnetic field, B, as a function of an applied external magnetic field, H, for different stress states [4]. The change in slope of the magnetization curves indicates the change in material permeability as a function of the part stress. The magnetoelastic relationship between stress and permeability of Galfenol is the physical principle underlying how a material can be used directly as a strain sensor. The center and right graphs of Figure 2 shows HRL's vibrating sample magnetometer (VSM) data for Galfenol and Monel respectively. The VSM data shows the internal magnetic field, B, as a function of the applied external field, H, for different temperature states. From the right graph, the change in the slope of the Monel magnetization curves is clearly a function of the applied temperature, while the center graph shows that the permeability of Galfenol is not sensitive to temperature changes. The thermomagnetic relationship between temperature and permeability of Monel is the physical principle underlying how a material can be used directly as a temperature sensor. The independence of Galfenol's permeability to temperature changes will limit the cross-coupling between the measured stress state and the applied temperature. However, as will be shown later, a coefficient

of thermal expansion mismatch between the parent material and Galfenol will produce a temperature induced strain measurement in the Galfenol.

The embedded Galfenol and Monel inclusions can be thought of as amplifying magnetic transducers for the internal stress state that is readable by standard eddy current inspection hardware. By reducing the embedded sensor to a material choice, the volume of the embedded sensing element can be minimized, reducing the impact on the structural part properties. One limitation of these materials, as shown in the Figure 2 data, is that their magnetization saturates, limiting the sensing range. We show later that we can measure temperature ranges from 0 ºC to 70 ºC and stresses from 0 to 70 MPa with an accuracy comparable to wired strain gauges and thermocouples. Thoughtful placement of the sensing materials within the stress and temperature fields of a part allows for using these limited sensing ranges to measure higher correlated stresses and temperatures at the potential point of failure. An example case is presented below where a sensor placed just off the neutral axis in a three-point-bend test specimen captures the onset of plasticity in high strength aluminum at approximately 462 MPa.

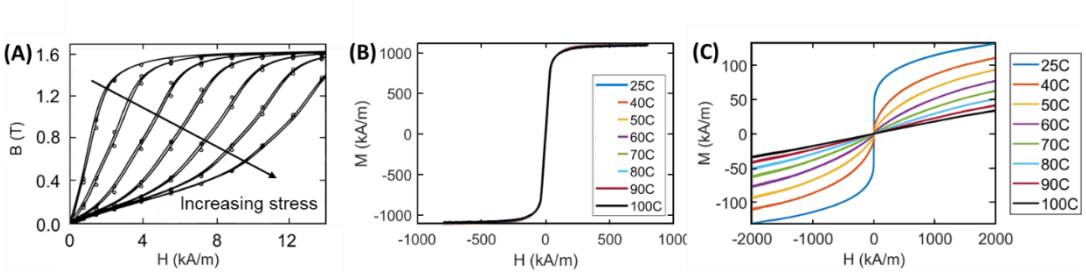

Figure 2. (A) Magnetoelastic behavior of Galfenol, showing changes in the material's permeability in response to stress. Figure sourced from [4]. (B) Vibrating sample magnetometer (VSM) measurements showing the thermal insensitivity of free-standing Galfenol's magnetic properties. (C) Vibrating sample magnetometer (VSM) measurements showing the thermal sensitivity of Monel's magnetic properties.

THE EMBEDDING PROCESS

Galfenol sensors with a square 0.5mm by 0.5mm cross-section and a length of 5mm were cut and ground from bar stock for strain measurements in the direction of their long axis. Monel wire with a 0.5mm diameter and 5mm length was selected for temperature measurements. The magneto-responsive materials were inserted into aluminum microtubes with 1mm outer diameter and 0.8mm inner diameter to protect them during the Laser Powder Bed Fusion 3D printing process. Figure 3A shows a Galfenol sensor inside an aluminum microtube. Because mechanical forces must be transduced from the parent material to the strain sensing element, the ends of the microtube capsules are crimped onto the Galfenol using pliers to form a firm mechanical connection between the two components. During 3D printing, cavities were created in areas selected for sensor embedding by not melting the powder in these regions. After interrupting the print process, the powder was loosened with a brush and blown away before sensing elements were manually placed in the cavities (Figure 3B). This sensor placement could be automated in production-scale applications. Next, a new layer of powder was spread and lased around the sensing elements to fuse the aluminum powder to the aluminum microtube capsules. This establishes a good mechanical and thermal connection between the sensor housing and the part (Figure 3C-D). High strength 7A77

aluminum alloy powder was used, and it is compatible with the aluminum microtube housing which shields the magneto-responsive materials from the laser and melt pool. The small size of the sensor limits its effect on the structural properties of the part, and the elliptical cavities can be strategically aligned to minimize the maximum stress along their boundary. Print parameters and void geometry can be further developed to reduce wall roughness and conform to the microtube exterior more precisely. This approach can be extended to other alloys, including titanium, nickel and steel, noting that the higher the melting point of the alloy, the more important it is for the sensor housing to protect the magneto-responsive materials.

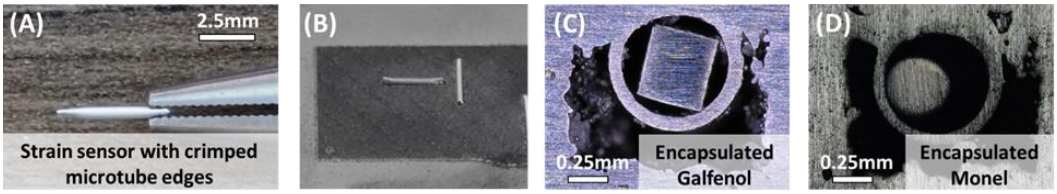

Figure 3. Process for embedding magneto-responsive sensing elements. (A) The magneto-responsive material is encapsulated in an aluminum microtube housing with crimped ends. (B) During 3D printing, several layers of powder are not melted in selected locations and subsequently the loose powder is removed to create cavities where the sensing elements are placed (shown). Next, another layer of powder is spread over the sensing elements, they are welded to the part by melting the powder around them and the print is continued, resulting in magneto-responsive inclusions. (C) A cross-section of an embedded Galfenol sensor and its protective capsule. (D) A cross-section of an embedded Monel sensor and its protective capsule.

SENSOR ACCURACY

The temperature and strain sensing accuracies are dependent on the volume of embedded magneto-responsive material, the embedding depth, coil design and magnetic field strength. Because the focus of this work is not on coil design and we use components that are readily available off-the-shelf for wireless, non-contact sensing, we provide an accuracy assessment that isolates the contribution of the magneto-responsive materials by wrapping copper wire around dog bone tensile coupons with 2.5 mm embedded sensing elements. Figure 4A shows that strain sensing is accurate to $\pm 27 \times 10^{-6}$ over at least a 6×10^{-4} strain range to a 95% confidence interval. This accuracy represents data collected over four loading and unloading cycles to 70MPa at $23^{o}\mathrm{C}$ and $40^{o}\mathrm{C}$, with the CTE mismatch correction factor $\sigma_{\Delta T} = E_{FeGa}(\alpha_{FeGa} - \alpha_p)\Delta T$ to overlay the data. This data was collected at thermal equilibrium inside an environmental chamber with a thermocouple adhered to the surface of the specimen. Figure 4B shows that temperature sensing is accurate to $\pm 0.75^{o}\mathrm{C}$ over a $70^{o}\mathrm{C}$ range, to a 95% confidence interval, with the inductance measurement calibrated to a thermocouple. These results are extended to a non-uniform stress field with externally mounted sensing coils in the next section, with the expected reduction in accuracy reported below.

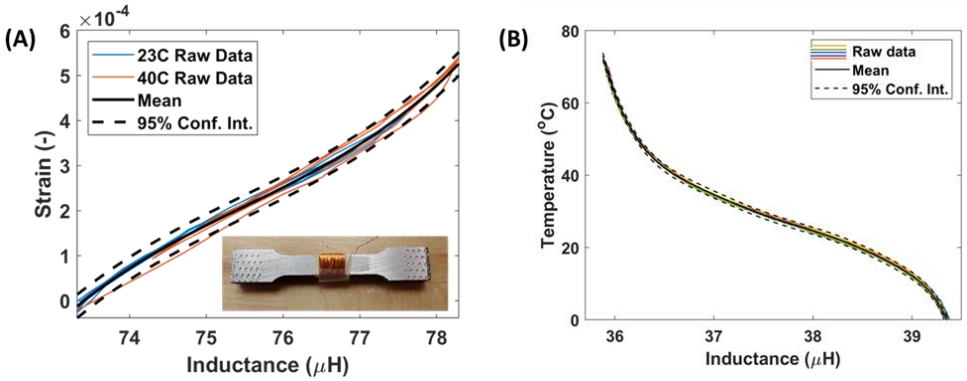

Figure 4. (A) Strain sensing is accurate to $\pm 27 \times 10^{-6}$ over a 6×10^{-4} strain range by wrapping copper wire around a dogbone tensile coupons with a Galfenol inclusion. The data was collected over four loading cycles at 23°C and four cycles at 40°C and aligned using an analytical CTE mismatch adjustment. (B) Temperature sensing is accurate to $\pm 0.75°C$ over a 70°C range**.** The data was collected over five heating and cooling cycles with a thermocouple embedded into the end of the sample and a copper coil wrapped around the test specimen to measure changes in permeability of the thermomagnetic inclusion. Both accuracy assessments are relative to a 95% confidence interval.

STRUCTURAL DAMAGE ASSESSMENT

As an initial demonstration of our ability to detect the onset of damage prior to part failure, a three-point bend specimen was 3D printed with 8 sensors, 4 strain sensors and 4 temperature sensors, embedded 2.0 mm deep. The test specimen is 8 mm thick with the strain sensors placed halfway between the neutral axis and the location of maximum stress on the outer surfaces of the part. Sensing coils were hand wound and mounted on the surface of the test specimen. As shown in Figure 5, the part with the sensing coils was cycled in a 3-point bend test fixture mounted within an Instron load frame. A strain gauge was placed on the test specimen to be used as a calibration data point for a finite element model of the test specimen. In Figure 5B, the strain gauge data for the test specimen with the embedded sensors is compared to strain gauge data for a baseline 3D printed test specimen without embedded sensors. The strain gauge failed for the embedded test specimen at about 9 kN while the embedded strain sensor continued to record strain up to the point of part failure at 11.5 kN, as shown in Figure 5C. The minor strain cycles measured in the embedded strain sensor clearly indicate the onset of plasticity at about 464.2 MPa, which indicates only a 5% reduction in yield strength relative to the baseline test specimen that failed at 488.2 MPa. All stresses were determined from calibrated finite element models of the tests. Using the calibrated models and inductance to force measurement calibration uncertainty, we estimate our embedded sensor accuracy to be $\pm 2.0 \times 10^{-4}$ strain.

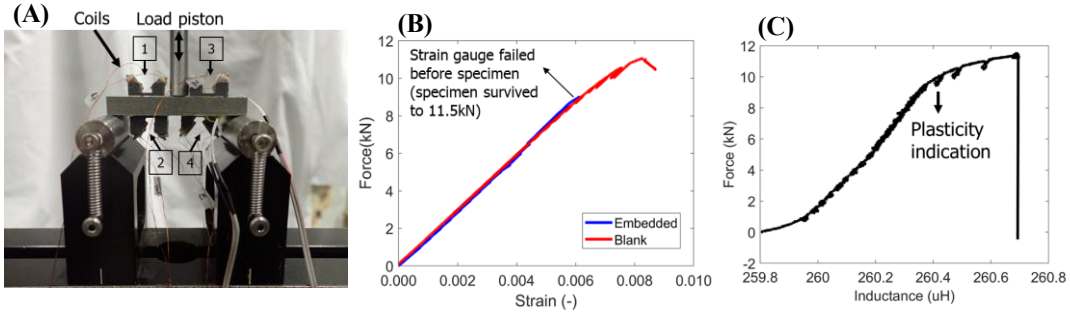

Figure 5. (A) 3D printed embedded sensor test specimen on an Instron load frame three-point bend test fixture with 4 pairs of sensing coils located in proximity to the 4 embedded Galfenol strain sensors (B) Strain gauge data for the embedded test specimen (blue) compared to the baseline test specimen (red) without any embedded sensors. (C). The embedded strain sensor data for the same test showing the onset of plasticity in the minor cycles prior to part failure at 11.5 kN, a 5% reduction in yield strength relative to the baseline test specimen.

CONCLUSION

In this paper we demonstrate wireless, embedded detection of the onset of plasticity in 3D printed metal parts using only material inclusions that can be remotely interrogated using eddy current inspection techniques. This result extends standard eddy current inspection methods to include stress and temperature measurements in difficult to reach locations. Our approach has the benefit of having a minimal impact on part structural properties because the only modification to the part is the embedding of small material inclusions whose magnetic properties can be remotely interrogated without the need to run wires through the part. We believe that the results are an important step toward in-situ structural health monitoring for maintenance on an as-needed basis with the goal of replacing the current practice of scheduled maintenance intervals with expensive tear-down damage inspections. Future work will extend these results to establish deeper embedding distances, the detection of cracks in low cycle fatigue tests, and the establishment of high cycle durability limits.

ACKNOWLEDGEMENTS

Funding was provided by HRL Laboratories, LLC and the Defense Advanced Research Programs Agency under the Structural Evaluation through Non-contact Sensor Embedding (DARPA SENSE) program (agreement number HR00112490321) managed by Dr. Andrew Detor. The authors gratefully acknowledge informative discussion with Geoff McKnight, Mark O'Masta, Lorenzo Valdevit, Alireza Kermani, Paul Witherell, and Kyle Rosenkoetter. The views, opinions and/or findings expressed are those of the authors and should not be interpreted as representing the official views or policies of the Department of Defense or the U.S. Government.

REFERENCES

1. "Nondestructive Evaluation Requirements for Fracture-Critical Metallic Components", NASA-STD-5009B, 2019-05-08.
2. "Integral part: A 3D-printing first, Chinook took 3D-printed, flight critical part for a spin during test flights – a helicopter first", Boeing Innovation Quarterly, 2022 Q2, Vol. 6, Iss. 20, pages 52-59.
3. J. H. Martin, B. D. Yahata, J. M. Hundley, J. A. Mayer, T. A. Schaedler and T. M. Pollock, "3D printing of high-strength aluminium alloys," Nature, vol. 549, pp. 365-369, 2017.
4. J. J. Scheidler, V. M. Asnani and M. J. Dapino, Dynamic characterization of Galfenol (Fe81. 6Ga18. 4), NASA/TP—2016-218754, 2016.